Appl. Math. Mech. -Engl. Ed., **42**(7), 981–998 (2021)

APPLIED MATHEMATICS AND MECHANICS (ENGLISH EDITION)

https://doi.org/10.1007/s10483-021-2747-9

Nonlinear vibration of functionally graded graphene platelet-reinforced composite truncated conical shell using first-order shear deformation theory*

Shaowu YANG[1], Yuxin HAO[1], Wei ZHANG[2,†], Li YANG[1], Lingtao LIU[1]

1. College of Mechanical Engineering, Beijing Information Science and Technology University, Beijing 100192, China;
2. Beijing Key Laboratory of Nonlinear Vibrations and Strength of Mechanical Structures, College of Mechanical Engineering, Beijing University of Technology, Beijing 100124, China

(Received Feb. 3, 2021 / Revised Apr. 24, 2021)

Abstract In this study, the first-order shear deformation theory (FSDT) is used to establish a nonlinear dynamic model for a conical shell truncated by a functionally graded graphene platelet-reinforced composite (FG-GPLRC). The vibration analyses of the FG-GPLRC truncated conical shell are presented. Considering the graphene platelets (GPLs) of the FG-GPLRC truncated conical shell with three different distribution patterns, the modified Halpin-Tsai model is used to calculate the effective Young's modulus. Hamilton's principle, the FSDT, and the von-Karman type nonlinear geometric relationships are used to derive a system of partial differential governing equations of the FG-GPLRC truncated conical shell. The Galerkin method is used to obtain the ordinary differential equations of the truncated conical shell. Then, the analytical nonlinear frequencies of the FG-GPLRC truncated conical shell are solved by the harmonic balance method. The effects of the weight fraction and distribution pattern of the GPLs, the ratio of the length to the radius as well as the ratio of the radius to the thickness of the FG-GPLRC truncated conical shell on the nonlinear natural frequency characteristics are discussed. This study culminates in the discovery of the periodic motion and chaotic motion of the FG-GPLRC truncated conical shell.

Key words nonlinear free vibration, harmonic balance method, functionally graded graphene platelet-reinforced composite (FG-GPLRC), truncated conical shell, chaos

Chinese Library Classification O322
2010 Mathematics Subject Classification 74H45, 74H60, 74H65

---

* Citation: YANG, S. W., HAO, Y. X., ZHANG, W., YANG, L., and LIU, L. T. Nonlinear vibration of functionally graded graphene platelet-reinforced composite truncated conical shell using first-order shear deformation theory. *Applied Mathematics and Mechanics* (*English Edition*), **42**(7), 981–998 (2021) https://doi.org/10.1007/s10483-021-2747-9

† Corresponding author, E-mail: sandyzhang0@yahoo.com

Project supported by the National Natural Science Foundation of China (Nos. 12002057, 11872127, and 11832002), the Scientific Research Project of Beijing Educational Committee (No. KM202111232023), and the Qin Xin Talents Cultivation Program, Beijing Information Science & Technology University (Nos. QXTCP C202102 and A201901)

1 Introduction

The outstanding material properties of graphene composites, e.g., excellent thermal, mechanical, physicochemical, and electronic properties, have attracted the attention of many researchers. For example, Young's modulus of graphene can be as high as 1 TPa, the ultimate strength can be as high as 130 GPa[1], the thermal conductivity is $5\,000\,\mathrm{W}\cdot\mathrm{m}^{-1}\cdot\mathrm{K}^{-1}$[2], and the electrical conductivity of graphene is $6\,000\,\mathrm{S}\cdot\mathrm{cm}^{-1}$[3]. Rafiee et al.[4] found that the critical buckling load of graphene-reinforced composite material is increased by 52% by adding 0.1% weight fraction of graphene sheets to an epoxy resin matrix. The conical shell is a well-known important structural unit in many engineering fields, e.g., rocket propulsion systems, aircraft, pressure, and piping vessels, and ship structures[5–6]. Because the graphene-reinforced composite conical shell structure has extensive application prospects in many engineering fields, it is necessary to predict and discover nonlinear vibration characteristics.

Researchers have increasingly paid attention to graphene-reinforced composite structures because of their exceptional mechanical properties. Yang and his group conducted numerous studies to assess the bending, vibration, and buckling of beam and plate structures of the functionally graded graphene platelet-reinforced composite (FG-GPLRC)[7–11]. Zhao et al.[12] reviewed recent studies dedicated to characterizing the mechanical and structural behavior of FG-GPLRC beams, plates, and shells with various loadings or boundary conditions, and discussed the challenges associated with and the future directions for FG-GPLRC structures. Shen et al.[13–14] studied the nonlinear vibration and postbuckling of an FG graphene reinforced composite cylindrical panel in thermal environments. The size-dependent postbuckling characteristics of FG-GPLRC multilayer microtubes containing initial geometrical imperfection were investigated by Lu et al.[15]. Their work could provide theoretical guidelines for the safety assessment and optimal design of GRC tubular structures. Yas and Rahimi[16] presented a study on the thermal vibration of FG porous nanocomposite beams reinforced by graphene platelets (GPLs) based on the Timoshenko beam theory. Blooriyan et al.[17] proposed an analytical approach to investigate the postbuckling behavior of FG GPL reinforced polymer composite circular cylindrical shells subject to lateral pressure and axial compression. Nguyen et al.[18] developed a computational approach to investigate the dynamic responses, free vibrations, and active control behavior of smart FG metal foam plates reinforced with GPLs. Gao et al.[19] derived the governing equations for the FG metal foam plates by using the Hamilton principle based on three different plate theories, and investigated the effects on the wave dispersion relations of the geometrical and material properties of the plates. Wang et al.[20] employed the Hamilton principle and the improved Donnell nonlinear shell theory to formulate a model for a metal foam cylindrical shell reinforced by GPLs and investigated the nonlinear vibration characteristics. Liu et al.[21] studied the free vibrations, forced vibrations, and transient responses of the GPLs-FG plates.

A number of papers have reported the investigations of the vibrational characteristics of conical shell structures. A review on the buckling and vibrational characteristics of functionally graded material (FGM) conical shells was published by Sofiyev[22]. Song et al.[23] studied the free vibration of the conical shells subject to an elastic constraint and inertia force under arbitrary boundary conditions. Based on the assumptions of uncoupled thermo-elasticity, Akbari et al.[24] analyzed the thermal vibrations of an FGM conical shell. Ansari et al.[25] employed the higher-order shear deformation shell theory to study the free vibrations and large-amplitude forced vibrations of a composite conical shell reinforced by FG carbon nanotubes. Chan et al.[26–27] investigated the nonlinear dynamic behavior of the truncated eccentrically stiffened FG conical shell and truncated FG conical panel. The Haar wavelet method was used to derive the frequencies of a truncated rotating conical shell[28]. Rahmani et al.[29] investigated the vibrations of temperature dependent sandwich truncated conical shells under various thermal conditions. Hao et al.[30–31] analyzed the nonlinear flutter characteristics of the truncated FG

conical panels and shells.

In the past few years, a large number of scholars have focused on the buckling and post-buckling behaviors of conical shell structures. The dynamic instability of the truncated FG conical shell and the FG orthotropic conical shell was studied by Deniz and Sofiyev[32] and Sofiyev et al.[33] who used the first-order shear deformation theory (FSDT). Hoa et al.[34] studied the nonlinear thermo-mechanical buckling and post-buckling behaviors of a truncated eccentric stiffener-FGM conical shell. The effects of the foundations, stiffeners, geometric dimensions, temperatures, and material properties on the stability of the truncated eccentric stiffener-FGM conical shell were determined. With the classical shell theory, Chan et al.[35–36] analyzed the nonlinear buckling of the truncated stiffened FG conical shell and a conical shell reinforced by FG carbon nanotubes under an axial compressive load. Kiani[37] conducted a buckling analysis for a composite laminated conical shell reinforced by graphene sheets. Jiao et al.[38] investigated the dynamic buckling behaviors of an FG carbon nanotube composite cylindrical shell subject to a dynamic displacement load by using a semi-analytical approach. Dung et al.[39] investigated the buckling characteristics of an imperfect thin conical plate subject to the simply supported condition. Bich et al.[40] studied the buckling characteristics of an FGM conical plate with external and axial loads.

To date, a large number of scholars have therefore analyzed the vibrational and buckling characteristics of conical shell structures. Nevertheless, few scholars have paid attention to graphene-reinforced composite truncated conical shell structures. This motivates our study, which involves nonlinear vibrational analyses of the FG-GPLRC truncated conical shell. Our study considers three distribution patterns of the GPLs in the FG-GPLRC truncated conical shell, and the effective Young's modulus is calculated by utilizing the modified Halpin-Tsai model. Based on the von-Karman nonlinear relations, FSDT, and Hamilton principle, we establish a dynamic model of the FG-GPLRC truncated conical shell, which can be expressed as ordinary differential equations via the Galerkin method. Then, the analytical nonlinear frequencies of the FG-GPLRC truncated conical shell are solved by using the harmonic balance method. The effects of the distribution pattern of the GPLs and the weight fraction, the ratio of the radius to the thickness as well as the ratio of the length to the radius of the FG-GPLRC truncated conical shell on the nonlinear vibrational behavior are discussed. This study leads to the discovery of the chaotic and periodic motions of the FG-GPLRC truncated conical shell.

2 Formulation of a model of the FG-GPLRC truncated conical shell

An FG-GPLRC truncated conical shell with the length L, the thickness h, the minor inner radius r_1, and the semi-vertex angle β is considered as shown in Fig. 1. In addition, the radius of the arbitrary point can be computed as $R = r_1 + x\sin\beta$ along the meridional direction. In Fig. 1, the curvilinear coordinate system (x, θ, z) is located on the mid-surface of the FG-GPLRC truncated conical shell along the axial, circumferential, and radial directions, respectively. The displacement components u, v, and w indicate the displacements of an arbitrary point of the FG-GPLRC truncated conical shell in the directions x, θ, and z, respectively. The transverse excitation $F\cos(\Omega t)$ is loaded on the outside surface of the FG-GPLRC truncated laminated conical shell along the z-direction.

GPLs are introduced into the truncated conical shell structures to improve the performance. Three different distribution patterns of the GPLs in the FG-GPLRC truncated conical shell are considered, namely, the GPL-U pattern, the GPL-X pattern, and the GPL-O pattern, as shown in Fig. 2. For the GPL-U pattern, the volume fractions of the GPLs maintain the same value along the thickness direction. The exterior and interior surfaces of the FG-GPLRC truncated conical shell are rich in the GPL-X pattern, whereas the GPL-O pattern prevails in the central region of the FG-GPLRC truncated conical shell, as shown in Fig. 2.

The volume fractions of the GPLs for the FG-GPLRC truncated conical shell change linearly

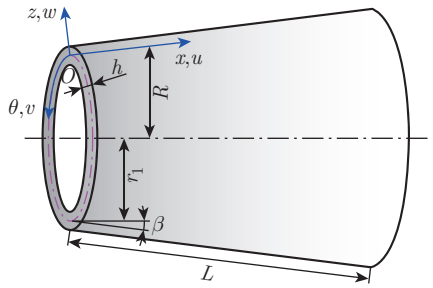

Fig. 1 Model and curvilinear coordinate system of an FG-GPLRC truncated conical shell (color online)

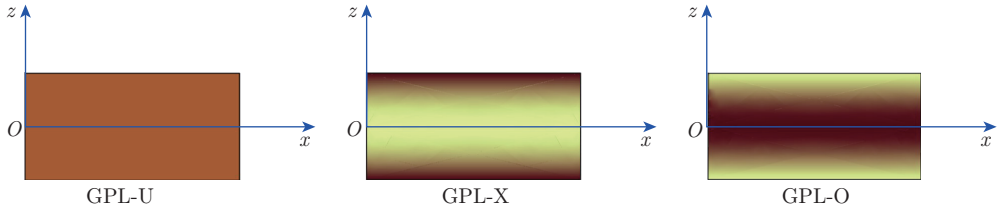

Fig. 2 Distribution patterns of three GPLs in FG-GPLRC materials (color online)

along the thickness direction[41], as shown in Fig. 3, and they are expressed as follows:

$$V_{\mathrm{GPL}} = \begin{cases} V^*, & \text{GPL-U}, \\ 2V^* \dfrac{2\,|z|}{h}, & \text{GPL-X}, \\ 2V^* \left(1 - \dfrac{2|z|}{h}\right), & \text{GPL-O}, \end{cases} \tag{1}$$

where V^* is the total volume fraction of the GPLs of the FG-GPLRC truncated conical shell, and can be obtained from the weight fraction of the GPLs W_{GPL} as follows:

$$V^* = \frac{W_{\mathrm{GPL}}}{W_{\mathrm{GPL}} + (1 - W_{\mathrm{GPL}})(\rho_{\mathrm{GPL}}/\rho_{\mathrm{M}})}, \tag{2}$$

in which ρ_{GPL} and ρ_{M} are the mass densities of the GPLs and the matrix, respectively.

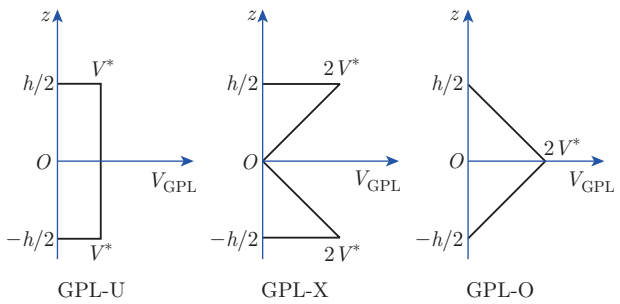

Fig. 3 Volume fractions of the GPLs for the FG-GPLRC truncated conical shell (color online)

The experiment proved that Young's modulus can be determined more accurately with the modified Halpin-Tsai model, and the rule of mixture enables the other properties to be computed accurately[42–43]. To reduce the amount of calculation and ensure calculation efficiency and accuracy, we use a modification of the Halpin-Tsai model for determining the effective Young's modulus, and the rule of mixture for the other properties.

According to the modified Halpin-Tsai model[43–44], the effective Young's modulus E of the FG-GPLRC truncated conical shell is assumed to be

$$E = \frac{3}{8}\frac{1+\xi_L\eta_L V_{\mathrm{GPL}}}{1-\eta_L V_{\mathrm{GPL}}}E_{\mathrm{M}} + \frac{5}{8}\frac{1+\xi_W\eta_W V_{\mathrm{GPL}}}{1-\eta_W V_{\mathrm{GPL}}}E_{\mathrm{M}} \tag{3}$$

with

$$\eta_L = \frac{\frac{E_{\mathrm{GPL}}}{E_{\mathrm{M}}}-1}{\frac{E_{\mathrm{GPL}}}{E_{\mathrm{M}}}+\xi_L}, \quad \eta_W = \frac{\frac{E_{\mathrm{GPL}}}{E_{\mathrm{M}}}-1}{\frac{E_{\mathrm{GPL}}}{E_{\mathrm{M}}}+\xi_W}, \tag{4a}$$

$$\xi_L = \frac{2l_{\mathrm{GPL}}}{h_{\mathrm{GPL}}}, \quad \xi_W = \frac{2w_{\mathrm{GPL}}}{h_{\mathrm{GPL}}}, \tag{4b}$$

where E_{M} is Young's modulus of the matrix, and E_{GPL}, h_{GPL}, w_{GPL}, and l_{GPL} are Young's modulus, thickness, width, and length of the GPLs, respectively.

The effective mass density ρ, the effective Poisson's ratio ν, and the coefficient of the thermal expansion α of the FG-GPLRC truncated conical shell are determined with the rule of mixture as follows:

$$\rho = \rho_{\mathrm{GPL}}V_{\mathrm{GPL}} + \rho_{\mathrm{M}}(1-V_{\mathrm{GPL}}), \tag{5}$$

$$\nu = \nu_{\mathrm{GPL}}V_{\mathrm{GPL}} + \nu_{\mathrm{M}}(1-V_{\mathrm{GPL}}), \tag{6}$$

$$\alpha = \alpha_{\mathrm{GPL}}V_{\mathrm{GPL}} + \alpha_{\mathrm{M}}(1-V_{\mathrm{GPL}}), \tag{7}$$

where ν_{GPL} and ν_{M} are Poisson's ratios of the GPLs and the matrix, respectively. The thermal expansion coefficient of the FG-GPLRC truncated conical shell does not change considerably over a certain temperature range[45–46]. Thus, we consider the thermal expansion coefficient to be constant.

According to the FSDT[47], the displacement fields of the FG-GPLRC truncated conical shell are assumed to be

$$u(x,\theta,z,t) = u_0(x,\theta,t) + z\varphi_x(x,\theta,t), \tag{8a}$$

$$v(x,\theta,z,t) = v_0(x,\theta,t) + z\varphi_\theta(x,\theta,t), \tag{8b}$$

$$w(x,\theta,z,t) = w_0(x,\theta,t), \tag{8c}$$

where u_0, v_0, and w_0 denote the mid-plane displacements in the x-, θ-, and z-directions, respectively. In addition, φ_x and φ_θ represent the rotations of the radial normal in the θ- and x-directions, respectively.

Substituting the displacement field equation (8) into the von Karman nonlinear strains-displacement relationships, the nonlinear strains of the FG-GPLRC truncated conical shell are rewritten as

$$\varepsilon_x = \frac{\partial u_0}{\partial x} + z\frac{\partial \varphi_x}{\partial x} + \frac{1}{2}\Big(\frac{\partial w_0}{\partial x}\Big)^2, \tag{9a}$$

$$\varepsilon_\theta = \Re\frac{\partial v_0}{\partial \theta} + z\Re\frac{\partial \varphi_\theta}{\partial \theta} + \Re w_0\cos\beta + \Re(u_0 + z\varphi_x)\sin\beta + \frac{1}{2}\Re^2\Big(\frac{\partial w_0}{\partial \theta}\Big)^2, \tag{9b}$$

$$\gamma_{x\theta} = \Re\frac{\partial u_0}{\partial \theta} + z\Re\frac{\partial \varphi_x}{\partial \theta} - \Re(v_0 + z\varphi_\theta)\sin\beta + \frac{\partial v_0}{\partial x} + z\frac{\partial \varphi_\theta}{\partial x} + \Re\frac{\partial w_0}{\partial x}\frac{\partial w_0}{\partial \theta}, \tag{9c}$$

$$\gamma_{\theta z} = \varphi_\theta + \Re\frac{\partial w_0}{\partial \theta} - \Re v_0\cos\beta, \tag{9d}$$

$$\gamma_{xz} = \frac{\partial w_0}{\partial x} + \varphi_x, \tag{9e}$$

where ε_x and ε_θ are the principal strains, and $\gamma_{x\theta}$, $\gamma_{\theta z}$, and γ_{xz} denote the shear strains. Furthermore, $\Re = 1/R$ in the above equations.

The temperature increment of the FG-GPLRC truncated conical shell in the radial direction varies linearly,

$$\Delta T(z) = T_{\mathrm{i}} + \frac{z}{h}(T_{\mathrm{o}} - T_{\mathrm{i}}), \tag{10}$$

where T_{o} represents the external temperature of the FG-GPLRC truncated conical shell, and T_{i} is the internal temperature.

The constitutive relation of the FG-GPLRC truncated conical shell is written as[42–43]

$$\begin{bmatrix}\sigma_x\\ \sigma_\theta\\ \sigma_{x\theta}\\ \sigma_{\theta z}\\ \sigma_{xz}\end{bmatrix} = \begin{bmatrix}Q_{11} & Q_{12} & 0 & 0 & 0\\ Q_{12} & Q_{22} & 0 & 0 & 0\\ 0 & 0 & Q_{66} & 0 & 0\\ 0 & 0 & 0 & Q_{44} & 0\\ 0 & 0 & 0 & 0 & Q_{55}\end{bmatrix}\left(\begin{bmatrix}\varepsilon_x\\ \varepsilon_\theta\\ \gamma_{x\theta}\\ \gamma_{\theta z}\\ \gamma_{xz}\end{bmatrix} - \begin{bmatrix}\alpha\\ \alpha\\ 0\\ 0\\ 0\end{bmatrix}\Delta T\right), \tag{11}$$

where Q_{ij} $(i, j = 1, 2, 4, 5, 6)$ represent the stiffness coefficients of the FG-GPLRC truncated conical shell, and they are denoted as

$$Q_{11} = Q_{22} = \frac{E}{1-\nu^2}, \quad Q_{12} = \frac{\nu E}{1-\nu^2}, \quad Q_{66} = Q_{44} = Q_{55} = \frac{E}{2(1+\nu)}. \tag{12}$$

Hamilton's principle is used to obtain the system of nonlinear partial differential equations of the FG-GPLRC truncated conical shell, which is expressed as

$$\int_{t_1}^{t_2}(\delta U - \delta K + \delta W)\mathrm{d}t = 0, \tag{13}$$

where δU and δK denote the virtual strain energy and virtual kinetic energy, respectively. The virtual strain energy δU is derived as follows:

$$\delta U = \int_0^{2\pi}\int_0^L\int_{-\frac{h}{2}}^{\frac{h}{2}}\left(\sigma_x\delta\varepsilon_x + \sigma_\theta\delta\varepsilon_\theta + \sigma_{\theta z}\delta\gamma_{\theta z} + \sigma_{zx}\delta\gamma_{zx} + \sigma_{x\theta}\delta\gamma_{x\theta}\right)R\mathrm{d}z\mathrm{d}x\mathrm{d}\theta. \tag{14}$$

The virtual kinetic energy δK is obtained as

$$\delta K = \int_0^{2\pi}\int_0^L\int_{-\frac{h}{2}}^{\frac{h}{2}}\rho\left(u\delta\dot{u} + v\delta\dot{v} + w\delta\dot{w}\right)R\mathrm{d}z\mathrm{d}x\mathrm{d}\theta. \tag{15}$$

The virtual work δW resulting from transverse excitation is expressed as

$$\delta W = \int_0^{2\pi}\int_0^L F\cos(\Omega t)\delta w R\mathrm{d}x\mathrm{d}\theta. \tag{16}$$

Substituting Eqs. (14)–(16) into Eq. (13) and utilizing Hamilton's principle enable a system of nonlinear partial differential equations of the FG-GPLRC truncated conical shell to be derived

as follows:

$$N_{xx,x} + \Re N_{x\theta,\theta} + \Re N_{xx}\sin\beta - \Re N_{\theta\theta}\sin\beta = I_0\ddot{u}_0 + I_1\ddot{\varphi}_x, \tag{17a}$$

$$N_{x\theta,x} + \Re N_{\theta\theta,\theta} + 2\Re N_{x\theta}\sin\beta + \Re Q_\theta\cos\beta = I_0\ddot{v}_0 + I_1\ddot{\varphi}_\theta, \tag{17b}$$

$$\begin{aligned} &Q_{x,x} + \Re Q_{\theta,\theta} + \Re Q_x\sin\beta - \Re N_{\theta\theta}\cos\beta + N_{xx,x}\frac{\partial w_0}{\partial x} + N_{xx}\frac{\partial^2 w_0}{\partial x^2} + \Re N_{xx}\frac{\partial w_0}{\partial x}\sin\beta \\ &+ \Re^2 N_{\theta\theta,\theta}\frac{\partial w_0}{\partial\theta} + \Re^2 N_{\theta\theta}\frac{\partial^2 w_0}{\partial\theta^2} + \Re N_{x\theta,\theta}\frac{\partial w_0}{\partial x} + 2\Re N_{x\theta,\theta}\frac{\partial^2 w_0}{\partial x\partial\theta} \\ &+ \Re N_{x\theta,x}\frac{\partial w_0}{\partial\theta} + F\cos(\Omega t) = I_0\ddot{w}_0, \end{aligned} \tag{17c}$$

$$M_{xx,x} + \Re M_{x\theta,\theta} - \Re Q_x + \Re M_{xx}\sin\beta - \Re M_{\theta\theta}\sin\beta = I_1\ddot{u}_0 + I_2\ddot{\varphi}_x, \tag{17d}$$

$$M_{x\theta,x} + \Re M_{\theta\theta,\theta} - \Re Q_\theta + 2\Re M_{x\theta}\sin\beta = I_1\ddot{v}_0 + I_2\ddot{\varphi}_\theta, \tag{17e}$$

where one overdot represents the first-order derivative with respect to time, and two overdots denote the second-order derivative. I_η is the mass moment of inertia, expressed as

$$I_\eta = \int_{-\frac{h}{2}}^{\frac{h}{2}} \rho z^\eta \mathrm{d}z, \quad \eta = 0, 1, 2. \tag{18}$$

The stress resultants and moment resultants of the FG-GPLRC truncated conical shell can be calculated as

$$\begin{cases} \begin{bmatrix} N_{xx} \\ N_{\theta\theta} \\ N_{x\theta} \end{bmatrix} = \int_{-\frac{h}{2}}^{\frac{h}{2}} [A, B] \begin{bmatrix} \varepsilon^{(0)} \\ \varepsilon^{(1)} \end{bmatrix} \mathrm{d}z + \begin{bmatrix} N_{xx}^{\mathrm{T}} \\ N_{\theta\theta}^{\mathrm{T}} \\ 0 \end{bmatrix}, \\ \begin{bmatrix} M_{xx} \\ M_{\theta\theta} \\ M_{x\theta} \end{bmatrix} = \int_{-\frac{h}{2}}^{\frac{h}{2}} [B, D] \begin{bmatrix} \varepsilon^{(0)} \\ \varepsilon^{(1)} \end{bmatrix} \mathrm{d}z + \begin{bmatrix} M_{xx}^{\mathrm{T}} \\ M_{\theta\theta}^{\mathrm{T}} \\ 0 \end{bmatrix}, \end{cases} \tag{19}$$

$$\begin{bmatrix} Q_x \\ Q_\theta \end{bmatrix} = K\int_{-\frac{h}{2}}^{\frac{h}{2}} A \begin{bmatrix} \gamma_{xz} \\ \gamma_{\theta z} \end{bmatrix} \mathrm{d}z, \tag{20}$$

$$\left(\begin{bmatrix} N_{xx}^{\mathrm{T}} \\ N_{\theta\theta}^{\mathrm{T}} \\ N_{x\theta}^{\mathrm{T}} \end{bmatrix}, \begin{bmatrix} M_{xx}^{\mathrm{T}} \\ M_{\theta\theta}^{\mathrm{T}} \\ M_{x\theta}^{\mathrm{T}} \end{bmatrix} \right) = \int_{z_k}^{z_{k+1}} \begin{bmatrix} Q_{11} & Q_{12} & 0 \\ Q_{12} & Q_{22} & 0 \\ 0 & 0 & Q_{66} \end{bmatrix} \begin{bmatrix} \alpha \\ \alpha \\ 0 \end{bmatrix} [\Delta T, \Delta T z] \mathrm{d}z, \tag{21}$$

where $K = 5/6$ is the shear correction coefficient.

In the above equations, the tensile rigidity A_{ij}, the bending-tensile coupling rigidity B_{ij}, and the bending rigidity D_{ij} of the FG-GPLRC truncated conical shell are expressed as

$$[A_{ij}, B_{ij}, D_{ij}] = \int_{-\frac{h}{2}}^{\frac{h}{2}} Q_{ij}[1, z, z^2]\mathrm{d}z, \quad i, j = 1, 2, 6, \tag{22}$$

$$A_{ij} = \int_{-\frac{h}{2}}^{\frac{h}{2}} Q_{ij}[1, z, z^2]\mathrm{d}z, \quad i, j = 4, 5. \tag{23}$$

Substituting Eqs. (17)–(23) into Eq. (16), the nonlinear partial differential governing equations can be expressed by the generalized displacements u_0, v_0, w_0, φ_x, and φ_θ of the FG-GPLRC truncated conical shell, as shown in Appendix A.

In this study, the boundary condition of the FG-GPLRC truncated conical shell is considered to be simply supported at both ends, and is expressed by

$$v_0 = w = N_x = M_x = M_{x\theta} = 0 \quad \text{at} \quad x = 0, L. \tag{24}$$

The displacements u_0, v_0, w_0, φ_x, and φ_θ of the FG-GPLRC truncated conical shell, which is subject to the simply supported boundary condition, are expressed as the double Fourier sine series,

$$u_0 = \sum_{m=1}^{M}\sum_{n=1}^{N} u_{mn}(t)\cos\left(\frac{m\pi x}{L}\right)\cos(n\theta), \tag{25a}$$

$$v_0 = \sum_{m=1}^{M}\sum_{n=1}^{N} v_{mn}(t)\sin\left(\frac{m\pi x}{L}\right)\sin(n\theta), \tag{25b}$$

$$w_0 = \sum_{m=1}^{M}\sum_{n=1}^{N} w_{mn}(t)\sin\left(\frac{m\pi x}{L}\right)\cos(n\theta), \tag{25c}$$

$$\varphi_x = \sum_{m=1}^{M}\sum_{n=1}^{N} \varphi_{xmn}(t)\cos\left(\frac{m\pi x}{L}\right)\sin(n\theta), \tag{25d}$$

$$\varphi_\theta = \sum_{m=1}^{M}\sum_{n=1}^{N} \varphi_{\theta mn}(t)\sin\left(\frac{m\pi x}{L}\right)\sin(n\theta), \tag{25e}$$

where $u_{mn}(t)$, $v_{mn}(t)$, $w_{mn}(t)$, $\varphi_{xmn}(t)$, and $\varphi_{\theta mn}(t)$ are the time varying coefficients, and m and n are the generatrix half wave and circumferential wave numbers, respectively.

The transverse excitation F can also be expanded as

$$F = \sum_{m=1}^{M}\sum_{n=1}^{N} f_{mn}(t)\sin\left(\frac{m\pi x}{L}\right)\sin(n\theta). \tag{25f}$$

The effects of the inertia terms of u_0, v_0, φ_x, and φ_θ on the nonlinear vibration characteristics of the FG-GPLRC truncated conical shell are much smaller than those of the radial inertia term[48–49]. Hence, the inertia terms u_0, v_0, φ_x, and φ_θ can be omitted from Eq. (16). Employing the Galerkin method and neglecting the inertia terms of u_0, v_0, φ_x, and φ_θ, the general rotation and in-plane displacements can be represented as functions of the transverse displacement. Furthermore, a system of second-order ordinary differential equations for the FG-GPLRC truncated conical shell can be yielded as

$$\ddot{w}_{mn} + \omega_{\mathrm{l}}^2 w_{mn} + \varsigma w_{mn}^3 = f_{mn}, \tag{26}$$

where ω_{l} is the linear natural frequency of the conical shell, and ς is the coefficient of the cubic term of the system. This system is the Duffing differential equation.

3 Harmonic balance method

In this section, the nonlinear natural frequency of the FG-GPLRC truncated conical shell is analyzed by using the harmonic balance method. For natural frequency analysis, the transverse excitation f_{mn} can be neglected. We assume the approximated periodic solution of the Duffing differential equation (26) as

$$w_{mn}(t) = A_0 + A_1\cos\psi, \tag{27}$$

where $\psi = \omega_{\mathrm{nl}}t + \beta_0$, in which ω_{nl} is the nonlinear natural frequency of the conical shell.

Introducing Eq. (27) into the Duffing differential equation (26) and combining the coefficients of the cosine functions yield the following equation:

$$\begin{aligned}&\omega_{\mathrm{l}} + \varsigma A_0^3 + \frac{3}{2}\varsigma A_0 A_1^2 + \left(\omega_{\mathrm{l}}A_1 - \omega_{\mathrm{nl}}^2 A_1 + 3\varsigma A_0^2 A_1 + \frac{3}{4}\varsigma A_1^2\right)\cos\psi\\ &+ \frac{3}{2}\varsigma A_0 A_1^2\cos(2\psi) + \frac{1}{4}\varsigma A_1^3\cos(3\psi) = 0.\end{aligned} \tag{28}$$

By using the harmonic balance method, setting the coefficients of the constant terms and $\cos\psi$ in Eq. (28) to zero, a series of algebraic equations can be obtained as follows:

$$\omega_{\mathrm{l}} + \varsigma A_0^3 + \frac{3}{2}\varsigma A_0 A_1^2 = 0, \tag{29a}$$

$$\omega_{\mathrm{l}} A_1 - \omega_{\mathrm{nl}}^2 A_1 + 3\varsigma A_0^2 A_1 + \frac{3}{4}\varsigma A_1^3 = 0. \tag{29b}$$

Compared with the amplitude A_1 of the FG-GPLRC truncated conical shell, the shift A_0 is very small. Thus, A_0^2 and A_0^3 in Eq. (29) can be neglected. For the nonlinear free vibration of the FG-GPLRC truncated conical shell, the initial condition provided in Eq. (26) can be set as follows:

$$w_{mn}\big|_{t=0} = w_{\max}, \quad \frac{\partial w_{mn}}{\partial t}\Big|_{t=0} = 0, \tag{30}$$

where $w_{\max}$ is the maximum amplitude of the FG-GPLRC truncated conical shell.

Setting $A_1 = w_{\max}$ in Eq. (29) to zero, the natural frequency of the FG-GPLRC truncated conical shell can be obtained as

$$\omega_{\mathrm{nl}} = \sqrt{\omega_{\mathrm{l}} + \frac{3}{4}\varsigma w_{\max}^2}. \tag{31}$$

Thus, the frequency ratio $\omega_{\mathrm{nl}}/\omega_{\mathrm{l}}$ of the FG-GPLRC truncated conical shell is indicated as

$$\omega_{\mathrm{nl}}/\omega_{\mathrm{l}} = \sqrt{1 + \frac{3}{4\omega_{\mathrm{l}}}\varsigma w_{\max}^2}. \tag{32}$$

4 Free vibrations

To evaluate the aforementioned formulations and the programs we developed, the dimensionless natural frequency $\Omega_{\mathrm{n}} = \omega_{\mathrm{n}} R\sqrt{(1-\nu^2)\rho/E}$ is calculated. The dimensionless natural frequency of the pure metal truncated conical shell and the results of Najafov and Sofiyev[50], Kerboua et al.[51], and Liew et al.[52] are compared in Table 1. The geometric relations ($\beta = \pi/6$, $R/h = 100$, and $L = 0.25R\sin\beta$) of the pure metal truncated conical shell are considered. Specifically, our results are in good agreement with the previous results in Refs. [50]–[52] for the pure metal truncated conical shell.

Table 1 Dimensionless natural frequency of the pure metal truncated conical shell

n	Najafov and Sofiyev[50]	Kerboua et al.[51]	Liew et al.[52]	Present study
2	0.794 3	0.790 9	0.790 4	0.792 2
3	0.708 5	0.728 2	0.727 4	0.708 9
4	0.619 9	0.634 9	0.633 9	0.635 7

The method proposed in this paper is validated by comparing the nonlinear to linear frequency ratios of an isotropic square plate. The geometrical parameters of the isotropic square plate are $a/b = 1$ and $a/h = 10$. It should be noted that these nonlinear to linear frequency ratios are in excellent agreement with the results in Refs. [53]–[54].

Table 2 Nonlinear to linear frequency ratios of an isotropic square plate

$w_{\max}/h$	0.2	0.4	0.6	0.8
Teng and Wang[53]	1.033	1.027	1.268	1.443
Chen et al.[54]	1.033	1.027	1.280	1.453
Present	1.033	1.027	1.268	1.443

4.1 Linear natural frequencies

In the following analysis, the FG-GPLRC truncated conical shell with a thickness of $h = 0.002$ m and a semi-vertex angle of $\beta = 30°$ is considered. The material properties of the GPLs and matrix are $E_{\mathrm{M}} = 3.0$ GPa, $\rho_{\mathrm{M}} = 1\,200$ kg/m^3, $\nu_{\mathrm{M}} = 0.34$, $E_{\mathrm{GPL}} = 1\,010$ GPa, $\rho_{\mathrm{GPL}} = 1\,060$ kg/m^3, and $\nu_{\mathrm{GPL}} = 0.186$. The geometries of the GPLs with $w_{\mathrm{GPL}} = 1.5$ μm, $h_{\mathrm{GPL}} = 1.5$ nm, and $l_{\mathrm{GPL}} = 2.5$ μm are utilized[42]. The temperature of the inner surfaces of the FG-GPLRC truncated conical shell is $T_{\mathrm{i}} = 300$ K. The thermal expansion coefficients are $\alpha_{\mathrm{GPL}} = 5 \times 10^{-6}\,\mathrm{K}^{-1}$ and $\alpha_{\mathrm{M}} = 60 \times 10^{-6}\,\mathrm{K}^{-1}$ [46].

Table 3 lists the linear natural frequencies of the FG-GPLRC truncated conical shell for the three GPL distribution patterns when the ratio of the radius to the thickness is $r_1/h = 50$, the ratio of the length to the radius is $L/R = 2$, and the weight fraction of the GPLs is $W_{\mathrm{GPL}} = 0.01\%$. Consequently, the linear natural frequencies of the FG-GPLRC truncated conical shell increase with an increase in both m and n for the three GPL distribution patterns. The minimum frequency appears when $m = 1$ and $n = 1$, and it is the fundamental natural frequency.

Table 3 Linear natural frequencies of the FG-GPLRC truncated conical shell

Pattern	n	$m = 1$	$m = 2$	$m = 3$	$m = 4$
GPL-U	1	33.475 6	49.527 6	70.259 8	110.248 7
	2	48.257 8	75.845 1	100.240 0	142.587 4
	3	63.568 9	93.165 4	125.956 0	191.235 0
	4	96.587 4	120.874 5	189.954 8	300.251 4
GPL-X	1	33.643 2	51.245 6	80.560 0	124.856 2
	2	51.263 8	78.254 1	107.895 2	151.874 2
	3	67.251 0	98.451 2	133.658 9	207.569 8
	4	102.365 1	127.512 0	201.125 4	312.237 8
GPL-O	1	33.141 2	47.523 6	65.231 4	103.256 4
	2	44.231 5	68.263 5	95.458 7	135.264 5
	3	58.263 5	85.264 8	120.587 9	185.689 5
	4	89.256 4	112.365 8	180.547 8	289.246 5

Figure 4 illustrates the effects of the temperatures of the outer surfaces and the weight fraction of GPLs on the fundamental natural frequency of the FG-GPLRC truncated conical shell for the three GPL distribution patterns. Three different colored lines represent three different GPL distribution patterns. The fundamental natural frequencies of the FG-GPLRC truncated conical shell are observed to increase significantly when the distribution pattern of the GPLs increases from 0 to 1%. In addition, the fundamental natural frequencies of the

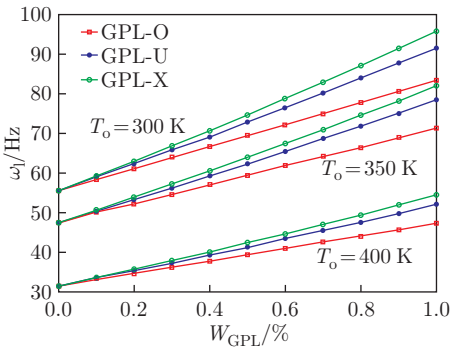

Fig. 4 Linear fundamental natural frequencies of the FG-GPLRC truncated conical shell (color online)

FG-GPLRC truncated conical shell change gradually as the distribution pattern of the GPLs changes. The GPL-X and GPL-O patterns give rise to the highest and lowest frequencies, respectively. The fundamental natural frequencies of the FG-GPLRC truncated conical shell of the GPL-U pattern are always between the highest and lowest values. The GPL-X pattern introduces the maximum stiffness to the system, whereas the GPL-O pattern results in the minimum stiffness of the system.

4.2 Nonlinear natural frequencies

This section presents our study of the nonlinear natural frequency of the FG-GPLRC truncated conical shells. This is based on Eq. (27), which is used to obtain the fundamental frequency ratio $\omega_{\mathrm{nl}}/\omega_{\mathrm{l}}$ of the FG-GPLRC truncated conical shell.

Figure 5 depicts the effects of the maximum amplitude of the FG-GPLRC truncated conical shell on the ratio of the nonlinear fundamental frequency to the linear fundamental frequency $\omega_{\mathrm{nl}}/\omega_{\mathrm{l}}$ with the distribution patterns of three GPLs. Figure 5 indicates that the ratio of the nonlinear fundamental frequency to the linear fundamental frequency $\omega_{\mathrm{nl}}/\omega_{\mathrm{l}}$ increases with an increase in the maximum amplitude of the FG-GPLRC truncated conical shell. However, for the three GPL distribution patterns, the order in which the ratio of the nonlinear fundamental frequency to the linear fundamental frequency $\omega_{\mathrm{nl}}/\omega_{\mathrm{l}}$ increases is as follows: GPL-O pattern > GPL-U pattern > GPL-X pattern.

Figure 6 shows the effects of the weight fraction of the GPLs W_{GPL} the FG-GPLRC truncated conical shell on the ratio of the nonlinear fundamental frequency to the linear fundamental frequency $\omega_{\mathrm{nl}}/\omega_{\mathrm{l}}$ with three GPL distribution patterns. Clearly, the ratio of the nonlinear fundamental frequency to the linear fundamental frequency $\omega_{\mathrm{nl}}/\omega_{\mathrm{l}}$ stays the same as the weight fraction of the GPLs increases. This is a highly interesting finding. As the weight fraction of the GPLs increases, the values of the fundamental nonlinear and linear frequencies increase simultaneously. Thus, the ratio of the nonlinear fundamental frequency to the linear fundamental frequency $\omega_{\mathrm{nl}}/\omega_{\mathrm{l}}$ remains almost the same.

The effects of the ratio of the radius to the thickness r_1/h of the FG-GPLRC truncated conical shell on the ratio of the nonlinear fundamental frequency to the linear fundamental frequency $\omega_{\mathrm{nl}}/\omega_{\mathrm{l}}$ are shown in Fig. 7. It is seen that the ratio of the nonlinear fundamental frequency to the linear fundamental frequency $\omega_{\mathrm{nl}}/\omega_{\mathrm{l}}$ increases as the ratio of the radius to the thickness r_1/h increases. In addition, this phenomenon exists in any of the GPL distribution patterns of the FG-GPLRC truncated conical shell. Figure 8 depicts the ratio of the nonlinear

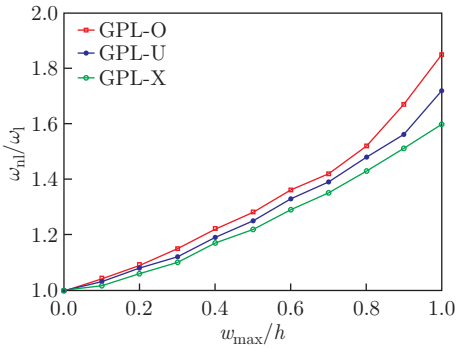

Fig. 5 Effects of the maximum amplitude of the FG-GPLRC truncated conical shell on the ratio of the nonlinear fundamental frequency to the linear fundamental frequency $\omega_{\mathrm{nl}}/\omega_{\mathrm{l}}$ (color online)

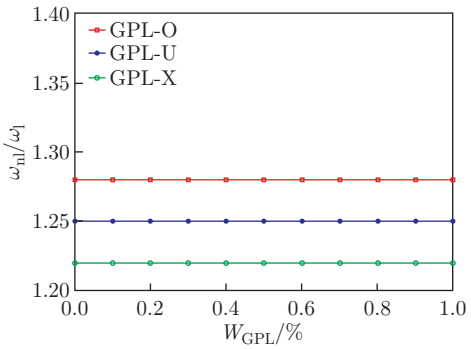

Fig. 6 Effects of the weight fraction of GPLs of the FG-GPLRC truncated conical shell on the ratio of the nonlinear fundamental frequency to the linear fundamental frequency $\omega_{\mathrm{nl}}/\omega_{\mathrm{l}}$ (color online)

fundamental frequency to the linear fundamental frequency $\omega_{\mathrm{nl}}/\omega_{\mathrm{l}}$ versus the ratio of the length to the radius L/r_1 of the FG-GPLRC truncated conical shell. For each of the GPL distribution patterns, the ratio of the nonlinear fundamental frequency to the linear fundamental frequency $\omega_{\mathrm{nl}}/\omega_{\mathrm{l}}$ decreases with the increase in the ratio of the length to the radius.

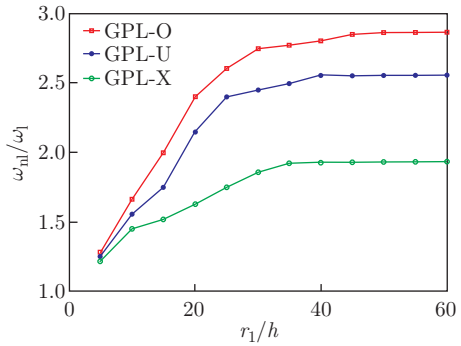

Fig. 7 Effects of the ratio of the radius to the thickness r_1/h of the FG-GPLRC truncated conical shell on the ratio of the nonlinear fundamental frequency to the linear fundamental frequency $\omega_{\mathrm{nl}}/\omega_{\mathrm{l}}$ (color online)

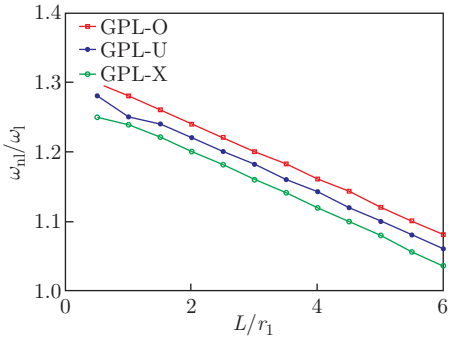

Fig. 8 Effects of the ratio of the length to the radius L/r_1 of the FG-GPLRC truncated conical shell on the ratio of the nonlinear fundamental frequency to the linear fundamental frequency $\omega_{\mathrm{nl}}/\omega_{\mathrm{l}}$ (color online)

5 Periodic and chaotic motions

This section presents the investigation of the nonlinear forced vibration of the FG-GPLRC truncated conical shell. To analyze both the chaotic and periodic motions of the system, the bifurcation diagram, the time history diagrams as well as the phase portraits are obtained by using the Runge-Kutta algorithm. For the first mode of the FG-GPLRC truncated conical shell, the initial condition of Eq. (26) is selected as $w_{11} = -0.001$ and $\dot{w}_{11} = -0.001$ in the following numerical simulation.

Figure 9 depicts the bifurcation diagram of the transverse excitation versus the amplitude of the first mode of the FG-GPLRC truncated conical shell with the GPL-U pattern when the transverse excitation increases from $f = 5 \times 10^5$ to $f = 10 \times 10^5$. This diagram enables us to visualize the chaotic and periodic motion of the FG-GPLRC truncated conical shell. In general, the motion law of the FG-GPLRC truncated conical shell that corresponds to an increase in the transverse excitation from $f = 5 \times 10^5$ to $f = 10 \times 10^5$ is given as chaotic motion $\rightarrow$

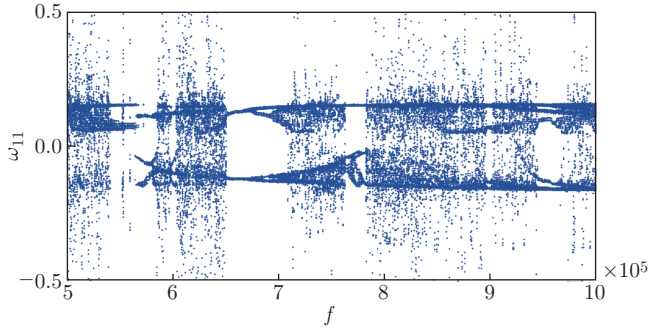

Fig. 9 Bifurcation diagram of the transverse excitation versus the amplitude of the first mode of the FG-GPLRC truncated conical shell (color online)

periodic motion → chaotic motion → periodic motion → chaotic motion → periodic motion → chaotic motion → periodic motion → chaotic motion. Thus, the periodic motion and chaotic motion alternate. However, a small chaotic window can be found in the periodic regions, with excitations such as $f = 5.496 \times 10^5$ and $f = 5.548 \times 10^5$. On the other hand, a small periodic window can be found in the chaotic regions with excitations such as $f = 6.083 \times 10^5$ and $f = 9.008 \times 10^5$. Thus, the nonlinear dynamic behavior of the FG-GPLRC truncated conical shell is highly complex.

The periodic motion (see Fig. 10) and chaotic motion (see Fig. 11) of the FG-GPLRC truncated conical shell are visually contrasted for different values of the transverse excitation ($f = 6.3 \times 10^5$ and $f = 6.6 \times 10^5$). Each of these figures includes the phase portrait and the time history diagram. The amplitude and velocity of the chaotic motion are larger than those of the periodic motion.

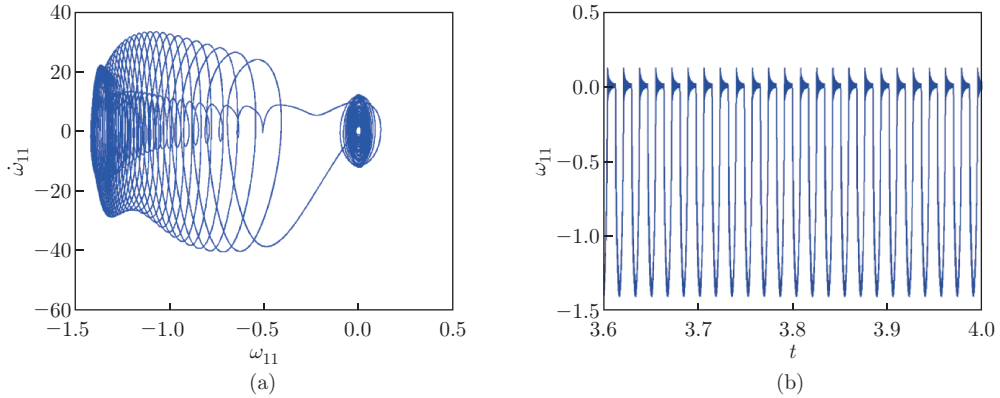

Fig. 10 Periodic motion of the FG-GPLRC truncated conical shell when $f = 6.3 \times 10^5$: (a) phase portrait and (b) time history diagram (color online)

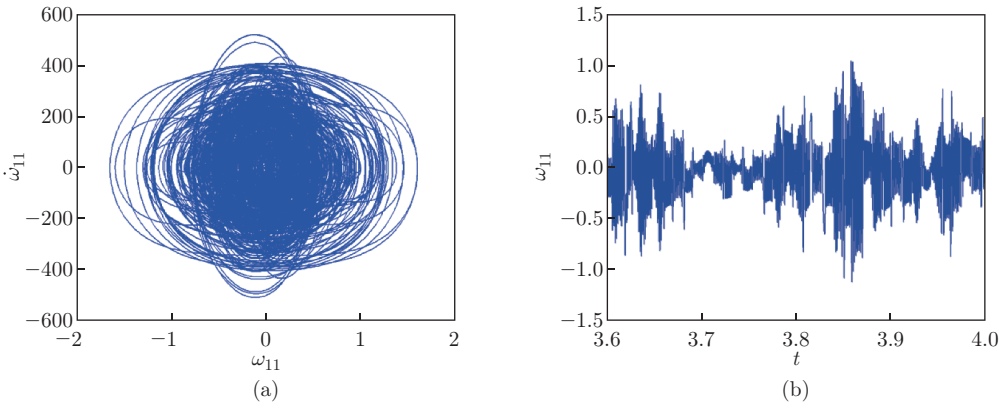

Fig. 11 Chaotic motion of the FG-GPLRC truncated conical shell when $f = 6.6 \times 10^5$: (a) phase portrait and (b) time history diagram (color online)

.

6 Conclusions

This study focuses on the analyses of the nonlinear vibrations of the FG-GPLRC truncated conical shell. Hamilton's principle, the FSDT, and the von-Karman type nonlinear geometric

relationship are used to derive a system of partial differential equations for the FG-GPLRC truncated conical shell. The ordinary differential equations of the FG-GPLRC truncated conical shell are obtained according to the Galerkin method. Then, the analytical nonlinear frequencies of the FG-GPLRC truncated conical shell are solved by utilizing the harmonic balance method. The proposed method is validated by comparing its performance with that of existing methods in the literature. A parametric study is proposed to assess the effects of the GPL weight fraction, the GPL distribution pattern, the ratio of the radius to the thickness, and the ratio of the length to the radius of the FG-GPLRC truncated conical shell on the nonlinear free vibration behavior. In addition, the chaotic and periodic motions of the FG-GPLRC truncated conical shell are discovered. It can be concluded as follows.

(i) The GPL distribution pattern, the weight fraction, the ratio of the radius to the thickness as well as the ratio of the length to the radius have significant effects on the free vibration characteristics of the FG-GPLRC truncated conical shell.

(ii) The GPL-X pattern maximizes while the GPL-O pattern minimizes the stiffness of the system.

(iii) An increase in the weight fraction of the GPLs is accompanied by a concomitant increase in the values of the fundamental nonlinear and linear frequencies, and the ratio of the fundamental nonlinear frequency to the linear frequency $\omega_{\mathrm{nl}}/\omega_{\mathrm{l}}$ remains almost the same.

(iv) The nonlinear dynamic behavior of the FG-GPLRC truncated conical shell is highly complex, and the periodic and chaotic motions are discovered.

References

[1] MAO, J. J. and ZHANG, W. Linear and nonlinear free and forced vibrations of graphene reinforced piezoelectric composite plate under external voltage excitation. *Composite Structures*, **203**, 551–565 (2018)

[2] SINGH, V., JOUNG, D., ZHAI, L., DAS, S., KHONDAKER, S. I., and SEAL, S. Graphene based materials: past, present and future. *Progress in Materials Science*, **56**, 1178–1271 (2011)

[3] MENSAH, B., GUPTA, K. C., KIM, H., WANG, W., JEONG, K., and NAH, C. Graphene-reinforced elastomeric nanocomposites: a review. *Polymer Testing*, **68**, 160–184 (2018)

[4] RAFIEE, M. A., RAFIEE, J., YU, Z. Z., and KORATKAR, N. Buckling resistant graphene nanocomposites. *Applied Physics Letters*, **95**, 223103 (2009)

[5] YANG, S. W., HAO, Y. X., ZHANG, W., and LI, S. B. Nonlinear dynamic behavior of functionally graded truncated conical shell under complex loads. *International Journal of Bifurcation and Chaos*, **25**(2), 1550025 (2015)

[6] YANG, S. W., ZHANG, W., HAO, Y. X., and NIU, Y. Nonlinear vibrations of FGM truncated conical shell under aerodynamics and in-plane force along meridian near internal resonances. *Thin-Walled Structures*, **142**, 369–391 (2019)

[7] YANG, J., WU, H., and KITIPORNCHAI, S. Buckling and postbuckling of functionally graded multilayer graphene platelet-reinforced composite beams. *Composite Structures*, **161**, 111–118 (2017)

[8] FENG, C., KITIPORNCHAI, S., and YANG, J. Nonlinear bending of polymer nanocomposite beams reinforced with non-uniformly distributed graphene platelets (GPLs). *Composites Part B: Engineering*, **110**, 132–140 (2017)

[9] SONG, M., YANG, J., and KITIPORNCHAI, S. Bending and buckling analyses of functionally graded polymer composite plates reinforced with graphene nanoplatelets. *Composites Part B: Engineering*, **134**, 106–113 (2018)

[10] WU, H., KITIPORNCHAI, S., and YANG, J. Thermal buckling and postbuckling of functionally graded graphene nanocomposite plates. *Materials & Design*, **132**, 431–441 (2017)

[11] SONG, M., LI, X., KITIPORNCHAI, S., BI, Q., and YANG, J. Low-velocity impact response of geometrically nonlinear functionally graded graphene platelet-reinforced nanocomposite plates. *Nonlinear Dynamics*, **95**(3), 2333–2352 (2019)

[12] ZHAO, S., ZHAO, Z., YANG, Z., KE, L. L., KITIPORNCHAI, S., and YANG, J. Functionally graded graphene reinforced composite structures: a review. *Engineering Structures*, **210**, 110339 (2020)

[13] SHEN, H. S., XIANG, Y., FAN, L., and HUI, D. Nonlinear vibration of functionally graded graphene-reinforced composite laminated cylindrical panels resting on elastic foundations in thermal environments. *Composites Part B*: *Engineering*, **136**, 177–186 (2018)

[14] SHEN, H. S., XIANG, Y., and FAN, L. Postbuckling of functionally graded graphene-reinforced composite laminated cylindrical panels under axial compression in thermal environments. *International Journal of Mechanical Sciences*, **135**, 398–409 (2018)

[15] LU, L., SHE, G. L., and GUO, X. Size-dependent postbuckling analysis of graphene reinforced composite microtubes with geometrical imperfection. *International Journal of Mechanical Sciences*, **199**, 106428 (2021)

[16] YAS, M. H. and RAHIMI, S. Thermal vibration of functionally graded porous nanocomposite beams reinforced by graphene platelets. *Applied Mathematics and Mechanics* (*English Edition*), **41**(8), 1209–1226 (2020) https://doi.org/10.1007/s10483-020-2634-6

[17] BLOORIYAN, S., ANSARI, R., DARVIZEH, A., GHOLAMI, R., and ROUHI, H. Post-buckling analysis of functionally graded graphene platelet-reinforced polymer composite cylindrical shells using an analytical solution approach. *Applied Mathematics and Mechanics* (*English Edition*), **40**(7), 1001–1016 (2019) https://doi.org/10.1007/s10483-019-2498-8

[18] NGUYEN, N. V., LEE, J., and NGUYEN-XUAN, H. Active vibration control of GPLs-reinforced FG metal foam plates with piezoelectric sensor and actuator layers. *Composites Part B*: *Engineering*, **172**, 769–784 (2019)

[19] GAO, W. L., QIN, Z. Y., and CHU, F. L. Wave propagation in functionally graded porous plates reinforced with graphene platelets. *Aerospace Science and Technology*, **102**, 105860 (2020)

[20] WANG, Y. Q., YE, C., and ZU, J. W. Nonlinear vibration of metal foam cylindrical shells reinforced with graphene platelets. *Aerospace Science and Technology*, **85**, 359–370 (2019)

[21] LIU, J., DENG, X., WANG, Q., ZHONG, R., XIONG, R., and ZHAO, J. A unified modeling method for dynamic analysis of GPL-reinforced FGP plate resting on Winkler-Pasternak foundation with elastic boundary conditions. *Composite Structures*, **244**, 112217 (2020)

[22] SOFIYEV. A. H. Review of research on the vibration and buckling of the FGM conical shells. *Composite Structures*, **211**, 301–317 (2019)

[23] SONG, Z. Y., CAO, Q. J., and DAI, Q. Y. Free vibration of truncated conical shells with elastic boundary constraints and added mass. *International Journal of Mechanical Sciences*, **155**, 286–294 (2019)

[24] AKBARI, M., KIANI, Y., and ESLAMI, M. R. Thermal buckling of temperature-dependent FGM conical shells with arbitrary edge supports. *Acta Mechanica*, **226**, 897–915 (2015)

[25] ANSARI, R., HASRATI, E., and TORABI, J. Nonlinear vibration response of higher-order shear deformable FG-CNTRC conical shells. *Composite Structures*, **222**, 110906 (2019)

[26] CHAN, D. Q., ANH, V. T. T., and DUC, N. D. Vibration and nonlinear dynamic response of eccentrically stiffened functionally graded composite truncated conical shells surrounded by an elastic medium in thermal environments. *Acta Mechanica*, **230**, 157–178 (2019)

[27] CHAN, D. Q., QUAN, T. Q., and KIM, S. E. Nonlinear dynamic response and vibration of shear deformable piezoelectric functionally graded truncated conical panel in thermal environments. *European Journal of Mechanics-A/Solids*, **77**, 103795 (2019)

[28] DAI, Q. Y., CAO, Q. J., and CHEN, Y. S. Frequency analysis of rotating truncated conical shells using the Haar wavelet method. *Applied Mathematical Modelling*, **57**, 603–613 (2018)

[29] RAHMANI, M., MOHAMMADI, Y., and KAKAVAND, F. Vibration analysis of sandwich truncated conical shells with porous FG face sheets in various thermal surroundings. *Steel and Composite Structures*, **32**, 239–252 (2019)

[30] HAO, Y. X., YANG, S. W., ZHANG, W., YAO, M. H., and WANG, A. W. Flutter of high-dimension nonlinear system for an FGM truncated conical shell. *Mechanics of Advanced Materials and Structures*, **25**, 47–61 (2018)

[31] HAO, Y. X., NIU, Y., ZHANG, W., LI, S. B., YAO, M. H., and WANG, A. W. Supersonic flutter analysis of FGM shallow conical panel accounting for thermal effects. *Meccanica*, **53**, 95–109 (2018)

[32] DENIZ, A. and SOFIYEV, A. H. The nonlinear dynamic buckling response of functionally graded truncated conical shells. *Journal of Sound and Vibration*, **332**, 978–992 (2013)

[33] SOFIYEV, A. H., ZERIN, Z., ALLAHVERDIEV, B. P., HUI, D., TURAN, F., and ERDEM, H. The dynamic instability of FG orthotropic conical shells within the SDT. *Steel and Composite Structures*, **25**, 581–591 (2017)

[34] HOA, L. K., HOAI, B. T. T., and CHAN, D. Q. Nonlinear thermomechanical postbuckling analysis of ES-FGM truncated conical shells resting on elastic foundations. *Mechanics of Advanced Materials and Structures*, **26**, 1089–1103 (2019)

[35] CHAN, D. Q., NGUYEN, P. D., and QUANG, V. D. Nonlinear buckling and post-buckling of functionally graded CNTs reinforced composite truncated conical shells subjected to axial load. *Steel and Composite Structures*, **31**, 243–259 (2019)

[36] CHAN, D. Q., LONG, V. D., and DUC, N. D. Nonlinear buckling and postbuckling of FGM shear-deformable truncated conical shells reinforced by FGM stiffeners. *Mechanics of Composite Materials*, **54**, 745–764 (2019)

[37] KIANI, Y. Buckling of functionally graded graphene reinforced conical shells under external pressure in thermal environment. *Composites Part B*: *Engineering*, **156**, 128–137 (2019)

[38] JIAO, P., CHEN, Z. P., and LI, Y. Dynamic buckling analyses of functionally graded carbon nanotubes reinforced composite (FG-CNTRC) cylindrical shell under axial power-law time-varying displacement load. *Composite Structures*, **220**, 784–797 (2019)

[39] DUNG, D. V., HOA, L. K., THUYET, B. T., and NGA, N. T. Buckling analysis of functionally graded material (FGM) sandwich truncated conical shells reinforced by FGM stiffeners filled inside by elastic foundations. *Applied Mathematics and Mechanics* (*English Edition*), **37**(7), 879–902 (2016) https://doi.org/10.1007/s10483-016-2097-9

[40] BICH, D. H., PHUONG, N. T., and TUNG, H. V. Buckling of functionally graded conical panels under mechanical loads. *Composite Structures*, **94**, 1379–1384 (2012)

[41] SAFARPOUR, M., GHABUSSI, A., EBRAHIMI, F., HABIBI, M., and SAFARPOUR, H. Frequency characteristics of FG-GPLRC viscoelastic thick annular plate with the aid of GDQM. *Thin-Walled Structures*, **150**, 106683 (2020)

[42] SHOKRIEH, M. M., GHOREISHI, S. M., and ESMKHANI, M. Toughening mechanisms of nanoparticle-reinforced polymers. *Woodhead Publishing Series in Composites Science and Engineering*, **2015**, 295–320 (2015)

[43] MAO, J. J. and ZHANG, W. Buckling and post-buckling analyses of functionally graded graphene reinforced piezoelectric plate subjected to electric potential and axial forces. *Composite Structures*, **216**, 332–405 (2019)

[44] NIU, Y., ZHANG, W., and GUO, X. Y. Free vibration of rotating pretwisted functionally graded composite cylindrical panel reinforced with graphene platelets. *European Journal of Mechanics-A/Solids*, **77**, 103798 (2019)

[45] MOJIRI, H. R. and JEDARI-SALAMI, S. Free vibration and dynamic transient response of functionally graded composite beams reinforced with graphene nanoplatelets (GPLs) resting on elastic foundation in thermal environment. *Mechanics Based Design of Structures and Machines* (2020) https://doi.org/10.1080/15397734.2020.1766492

[46] DONG, Y., LI, X., GAO, K., LI, Y., and YANG, J. Harmonic resonances of graphene-reinforced nonlinear cylindrical shells: effects of spinning motion and thermal environment. *Nonlinear Dynamics*, **99**(2), 981–1000 (2020)

[47] REDDY, J. N. *Mechanics of Laminated Composite Plates and Shells*: *Theory and Analysis*, CRC Press, New York (2004)

[48] NOSEIR, A. and REDDY, J. N. A study of non-linear dynamic equations of higher-order deformation plate theories. *International Journal of Non-Linear Mechanics*, **26**(2), 233–249 (1991)

[49] TENG, M. W. and WANG, Y. Q. Nonlinear free vibration of rectangular plates reinforced with 3D graphene foam: approximate analytical solution. *Results in Physics*, **17**, 103147 (2020)

[50] NAJAFOV, A. M. and SOFIYEV, A. H. The non-linear dynamics of FGM truncated conical shells surrounded by an elastic medium. *International Journal of Mechanical Sciences*, **66**, 33–44 (2013)

[51] KERBOUA, Y., LAKIS, A. A., and HMILA, M. Vibration analysis of truncated conical shells subjected to flowing fluid. *Applied Mathematical Modelling*, **34**(3), 791–809 (2010)

[52] LIEW, K. M., NG, T. Y., and ZHAO, X. Free vibration analysis of conical shells via the element-free kp-Ritz method. *Journal of Sound and Vibration*, **281**, 627–645 (2005)

[53] TENG, M. W. and WANG, Y. Q. Nonlinear free vibration of rectangular plates reinforced with 3D graphene foam: approximate analytical solution. *Results in Physics*, **17**, 103147 (2020)

[54] CHEN, C. S., CHENG, W. S., CHIEN, R. D., and DONG, J. L. Large amplitude vibration of an initially stressed cross ply laminated plates. *Applied Acoustic*, **63**, 939–956 (2002)

Appendix A

The nonlinear equations of motion are expressed by the generalized displacements of the FG-GPLRC truncated conical shell as follows:

$$
\begin{aligned}
&A_{11}\frac{\partial^2 u_0}{\partial x^2}+\Re^2 A_{66}\frac{\partial^2 u_0}{\partial \theta^2}+\Re A_{11}\frac{\partial u_0}{\partial x}\sin\beta-\Re^2 A_{22}u_0\cos^2\beta+\Re\left(A_{12}+A_{66}\right)\frac{\partial^2 v_0}{\partial x\partial\theta}\\
&-\Re^2\left(A_{22}+A_{66}\right)\frac{\partial v_0}{\partial\theta}\sin\beta+\Re^2 A_{66}\frac{\partial^2 w_0}{\partial\theta^2}\frac{\partial w_0}{\partial x}+\Re^2\left(A_{12}+A_{66}\right)\frac{\partial^2 w_0}{\partial x\partial\theta}\frac{\partial w_0}{\partial\theta}+\Re N_{xx}^{\mathrm{T}}\sin\beta\\
&+2\Re\left(A_{11}-A_{12}\right)\frac{\partial^2 w_0}{\partial x^2}\sin\beta-2\Re^3\left(A_{12}-A_{22}\right)\frac{\partial^2 w_0}{\partial\theta^2}\sin\beta+\Re A_{12}\frac{\partial w_0}{\partial x}\cos\beta-\Re N_{\theta\theta}^{\mathrm{T}}\sin\beta\\
&-\Re^2 A_{22}w_0\sin\beta\cos\beta+B_{11}\frac{\partial^2\varphi_x}{\partial x^2}+\Re^2 B_{66}\frac{\partial^2\varphi_x}{\partial\theta^2}+\Re B_{11}\frac{\partial\varphi_x}{\partial x}\sin\beta-\Re^2 B_{22}\varphi_x\sin^2\beta\\
&-\Re^2\left(B_{22}+B_{66}\right)\frac{\partial\varphi_\theta}{\partial\theta}\sin\beta+\Re\left(B_{12}+B_{66}\right)\frac{\partial^2\varphi_\theta}{\partial x\partial\theta}+A_{11}\frac{\partial^2 w_0}{\partial x^2}\frac{\partial w_0}{\partial x}=I_0\ddot{u}_0+I_1\ddot{\varphi}_x,
\end{aligned}
\tag{A1}
$$

$$
\begin{aligned}
&\Re\left(A_{12}+A_{66}\right)\frac{\partial^2 u_0}{\partial x\partial\theta}+\Re^2\left(A_{22}+A_{66}\right)\frac{\partial u_0}{\partial\theta}\sin\beta+A_{66}\frac{\partial^2 v_0}{\partial x^2}+\Re^2 A_{22}\frac{\partial^2 v_0}{\partial\theta^2}\\
&-\Re^2\left(KA_{44}\cos^2\beta+A_{66}\sin^2\beta\right)v_0+\Re A_{66}\frac{\partial w_0}{\partial\theta}\frac{\partial^2 w_0}{\partial x^2}+\Re^3 A_{22}\frac{\partial^2 w_0}{\partial\theta^2}\frac{\partial w_0}{\partial\theta}+\Re A_{66}\frac{\partial v_0}{\partial x}\sin\beta\\
&+\Re\left(A_{12}+A_{66}\right)\frac{\partial^2 w_0}{\partial x\partial\theta}\frac{\partial w_0}{\partial x}+\Re^2 A_{66}\frac{\partial w_0}{\partial\theta}\frac{\partial w_0}{\partial x}\sin\beta+\Re^2 A_{22}\frac{\partial w_0}{\partial\theta}\cos\beta\\
&+\Re\left(B_{12}+B_{66}\right)\frac{\partial^2\varphi_x}{\partial x\partial\theta}+\Re^2\left(B_{22}+B_{66}\right)\frac{\partial\varphi_x}{\partial\theta}\sin\beta+\Re B_{66}\frac{\partial\varphi_\theta}{\partial x}\sin\beta+\Re B_{22}\frac{\partial^2\varphi_\theta}{\partial\theta^2}\\
&+\Re^2 KA_{44}\frac{\partial w_0}{\partial\theta}\cos\beta+\left(\Re KA_{44}\cos\beta-\Re^2 B_{66}\sin^2\beta\right)\varphi_\theta=I_0\ddot{v}_0+I_1\ddot{\varphi}_\theta,
\end{aligned}
\tag{A2}
$$

$$
\begin{aligned}
&2\Re^2 B_{66}\frac{\partial^2 w_0}{\partial x\partial\theta}\frac{\partial\varphi_x}{\partial\theta}+0.5\Re^2 A_{11}\left(\frac{\partial w_0}{\partial x}\right)^3\sin\beta-\Re N_{\theta\theta}^{\mathrm{T}}\cos\beta+\Re\left(B_{11}+B_{22}\right)\frac{\partial\varphi_x}{\partial x}\frac{\partial w_0}{\partial x}\\
&-\Re^2 A_{66}\frac{\partial v_0}{\partial\theta}\frac{\partial w_0}{\partial x}\sin\beta-\Re^3\left(A_{12}+A_{66}\right)\frac{\partial^2 w_0}{\partial\theta^2}\frac{\partial w_0}{\partial x}+2\Re^2\left(A_{12}+2A_{66}\right)\frac{\partial^2 w_0}{\partial x\partial\theta}\frac{\partial w_0}{\partial\theta}\frac{\partial w_0}{\partial x}\\
&-\Re^2 B_{66}\frac{\partial\varphi_\theta}{\partial x}\frac{\partial w_0}{\partial x}\sin\beta+A_{11}\frac{\partial^2 u_0}{\partial x^2}\frac{\partial w_0}{\partial x}+B_{11}\frac{\partial^2\varphi_x}{\partial x^2}\frac{\partial w_0}{\partial x}+\Re\left(A_{12}+A_{66}\right)\frac{\partial^2 v_0}{\partial x\partial\theta}\frac{\partial w_0}{\partial x}\\
&+\Re\left(B_{12}+B_{66}\right)\frac{\partial^2\varphi_\theta}{\partial x\partial\theta}\frac{\partial w_0}{\partial x}+\Re^2 A_{66}\frac{\partial^2 u_0}{\partial\theta^2}\frac{\partial w_0}{\partial x}+\Re(KA_{55}+N_{xx}^{\mathrm{T}})\frac{\partial w_0}{\partial x}\sin\beta
\end{aligned}
$$

$$
\begin{aligned}
&+\frac{3}{2}A_{11}\frac{\partial^2 w_0}{\partial x^2}\Big(\frac{\partial w_0}{\partial x}\Big)^2+0.5\Re^2\left(A_{12}+2A_{66}\right)\frac{\partial^2 w_0}{\partial\theta^2}\Big(\frac{\partial w_0}{\partial x}\Big)^2+0.5\Re^2A_{12}\Big(\frac{\partial w_0}{\partial x}\Big)^2\cos\beta\\
&+\Re\left(A_{11}+A_{12}\right)\frac{\partial w_0}{\partial x}\frac{\partial u_0}{\partial x}\sin\beta+\Re^2A_{12}\frac{\partial^2 w_0}{\partial\theta^2}\frac{\partial u_0}{\partial x}-A_{12}\frac{\partial u_0}{\partial x}\cos\beta+A_{11}\frac{\partial^2 w_0}{\partial x^2}\frac{\partial u_0}{\partial x}\\
&+2\Re A_{66}\frac{\partial^2 w_0}{\partial x\partial\theta}\frac{\partial v_0}{\partial x}-\Re^2A_{66}\frac{\partial w_0}{\partial\theta}\frac{\partial v_0}{\partial x}+\Re A_{12}\frac{\partial^2 w_0}{\partial x^2}w_0\cos\beta+\Re^3A_{22}\frac{\partial^2 w_0}{\partial\theta^2}w_0\cos\beta\\
&-\Re^2A_{22}w_0\cos\beta+\Re B_{12}\frac{\partial^2 w_0}{\partial x^2}\varphi_x\sin\beta+\Re^3B_{22}\frac{\partial^2 w_0}{\partial\theta^2}\varphi_x\sin\beta+0.5\Re^3A_{22}\frac{\partial^2 w_0}{\partial\theta^2}\cos\beta\\
&+\left(\Re KA_{55}-\Re^2B_{22}\cos\beta\right)\varphi_x\sin\beta+\Re^3B_{66}\frac{\partial w_0}{\partial\theta}\varphi_\theta\sin^2\beta-\Re^2B_{66}\frac{\partial^2 w_0}{\partial x\partial\theta}\varphi_\theta\sin\beta\\
&+\Re^3A_{22}\frac{\partial^2 w_0}{\partial\theta^2}u_0\sin\beta-\Re^3A_{22}u_0\sin\beta\cos\beta+\Re^2A_{12}\frac{\partial^2 w_0}{\partial x^2}u_0\sin\beta+\left(KA_{55}+N_{xx}^{\mathrm{T}}\right)\frac{\partial^2 w_0}{\partial x^2}\\
&+\Re^3A_{66}\frac{\partial w_0}{\partial\theta}v_0\sin^2\beta-2\Re^2A_{66}\frac{\partial^2 w_0}{\partial x\partial\theta}v_0\sin\beta+\Re^2\left(KA_{44}+N_{\theta\theta}^{\mathrm{T}}\right)\frac{\partial^2 w_0}{\partial\theta^2}+\Re B_{66}\frac{\partial^2\varphi_\theta}{\partial x^2}\frac{\partial w_0}{\partial\theta}\\
&+\Re^3\left(B_{22}-B_{66}\right)\frac{\partial\varphi_x}{\partial\theta}\frac{\partial w_0}{\partial\theta}+\Re A_{66}\frac{\partial^2 v_0}{\partial x^2}\frac{\partial w_0}{\partial\theta}+0.5\Re\left(A_{12}+2A_{66}\right)\frac{\partial^2 w_0}{\partial x^2}\Big(\frac{\partial w_0}{\partial\theta}\Big)^2\\
&+\Re^2\left(B_{12}+B_{66}\right)\frac{\partial^2\varphi_x}{\partial x\partial\theta}\frac{\partial w_0}{\partial\theta}+\Re^3A_{66}\frac{\partial^2 v_0}{\partial\theta^2}\frac{\partial w_0}{\partial\theta}+\Re^3B_{22}\frac{\partial^2\varphi_\theta}{\partial\theta^2}\frac{\partial w_0}{\partial\theta}+2\Re^3A_{66}\frac{\partial^2 w_0}{\partial x\partial\theta}\frac{\partial u_0}{\partial\theta}\\
&+0.5\Re^3A_{22}\frac{\partial^2 w_0}{\partial\theta^2}\Big(\frac{\partial w_0}{\partial\theta}\Big)^2+\Re A_{12}\frac{\partial^2 w_0}{\partial x^2}\frac{\partial v_0}{\partial\theta}+\Re^3A_{22}\frac{\partial^2 w_0}{\partial\theta^2}\frac{\partial v_0}{\partial\theta}+KA_{55}\frac{\partial\varphi_x}{\partial x}\\
&-\Re^2\left(KA_{44}+A_{22}\right)\frac{\partial v_0}{\partial\theta}\cos\beta+B_{11}\frac{\partial^2 w_0}{\partial x^2}\frac{\partial\varphi_x}{\partial x}-\Re B_{12}\frac{\partial\varphi_x}{\partial x}\cos\beta+\Re^2B_{12}\frac{\partial^2 w_0}{\partial\theta^2}\frac{\partial\varphi_x}{\partial x}\\
&+2\Re B_{66}\frac{\partial^2 w_0}{\partial x\partial\theta}\frac{\partial\varphi_\theta}{\partial x}-\Re^2B_{66}\frac{\partial w_0}{\partial\theta}\frac{\partial\varphi_\theta}{\partial x}\sin\beta+\Re^3\left(A_{22}-A_{66}\right)\frac{\partial w_0}{\partial\theta}\frac{\partial u_0}{\partial\theta}\sin\beta\\
&+\Re^2B_{66}\frac{\partial^2\varphi_x}{\partial\theta^2}\frac{\partial w_0}{\partial x}+\Re^2\left(A_{12}+A_{66}\right)\frac{\partial^2 u_0}{\partial x\partial\theta}\frac{\partial w_0}{\partial\theta}+F\cos\left(\Omega t\right)=I_0\ddot{w}_0,
\end{aligned}
\tag{A3}
$$

$$
\begin{aligned}
&B_{11}\frac{\partial^2 u_0}{\partial x^2}+\Re^2B_{66}\frac{\partial^2 u_0}{\partial\theta^2}+\Re B_{11}\frac{\partial u_0}{\partial x}\sin\beta-\Re^2B_{22}u_0\sin^2\beta+\Re\left(B_{12}+B_{66}\right)\frac{\partial^2 v_0}{\partial x\partial\theta}+\Re^2D_{66}\frac{\partial^2\varphi_x}{\partial\theta^2}\\
&-\Re^2\left(B_{22}+B_{66}\right)\frac{\partial v_0}{\partial\theta}\sin\beta+0.5\Re^2\left(B_{11}-B_{12}\right)\frac{\partial^2 w_0}{\partial x^2}\sin\beta-\Re^2B_{22}w_0\sin\beta\cos\beta+D_{11}\frac{\partial^2\varphi_x}{\partial x^2}\\
&+\Re B_{12}\frac{\partial w_0}{\partial x}\cos\beta+B_{11}\frac{\partial^2 w_0}{\partial x^2}\frac{\partial w_0}{\partial x}+\Re^2B_{66}\frac{\partial^2 w_0}{\partial\theta^2}\frac{\partial w_0}{\partial x}-KA_{55}\frac{\partial w_0}{\partial x}+\Re\left(D_{12}+D_{66}\right)\frac{\partial^2\varphi_x}{\partial x\partial\theta}\\
&-0.5\Re^2\left(B_{12}+B_{22}\right)\frac{\partial^2 w_0}{\partial\theta^2}\sin\beta+\Re^2\left(B_{12}+B_{66}\right)\frac{\partial^2 w_0}{\partial x\partial\theta}\frac{\partial w_0}{\partial\theta}-\Big(KA_{55}+\frac{1}{R^2}D_{22}\Big)\varphi_x\\
&+\Re D_{11}\frac{\partial\varphi_x}{\partial x}\sin\beta-\Re^2\left(D_{22}+D_{66}\right)\frac{\partial\varphi_\theta}{\partial\theta}\sin\beta+\Re M_{xx}^{\mathrm{T}}\sin\beta-\Re M_{\theta\theta}^{\mathrm{T}}\sin\beta=I_1\ddot{u}_0+I_2\ddot{\varphi}_x,
\end{aligned}
\tag{A4}
$$

$$
\begin{aligned}
&\Re\left(B_{12}+B_{66}\right)\frac{\partial^2 u_0}{\partial x\partial\theta}+\Re^2\left(B_{22}+B_{66}\right)\frac{\partial u_0}{\partial\theta}\sin\beta+B_{66}\frac{\partial^2 v_0}{\partial x^2}+\Re B_{66}\frac{\partial^2 w_0}{\partial x^2}\frac{\partial w_0}{\partial\theta}+\Re^3B_{22}\frac{\partial^2 w_0}{\partial\theta^2}\frac{\partial w_0}{\partial\theta}\\
&+\left(\Re KA_{44}\cos\beta-\Re^2B_{66}\sin^2\beta\right)v_0+\Re^2B_{66}\frac{\partial w_0}{\partial x}\frac{\partial w_0}{\partial\theta}\sin\beta+\left(\Re^2B_{22}\cos\beta-\Re KA_{44}\right)\frac{\partial w_0}{\partial\theta}\\
&+\Re^2\left(D_{22}+D_{66}\right)\frac{\partial\varphi_\theta}{\partial\theta}+\Re^2D_{22}\frac{\partial^2\varphi_\theta}{\partial\theta^2}+\Re D_{66}\frac{\partial\varphi_\theta}{\partial x}-\left(KA_{44}+\Re^2D_{66}\sin^2\beta\right)\varphi_\theta+\Re^2B_{22}\frac{\partial^2 v_0}{\partial\theta^2}\\
&+\Re B_{66}\frac{\partial v_0}{\partial x}\sin\beta+\Re\left(B_{12}+B_{66}\right)\frac{\partial^2 w_0}{\partial x\partial\theta}\frac{\partial w_0}{\partial x}+\Re\left(D_{12}+D_{66}\right)\frac{\partial^2\varphi_x}{\partial x\partial\theta}+D_{66}\frac{\partial^2\varphi_\theta}{\partial x^2}\\
=&I_1\ddot{v}_0+I_2\ddot{\varphi}_\theta.
\end{aligned}
\tag{A5}
$$